

IMA Journal of Applied Mathematics (2005) 1–27
doi: 10.1093/imamat/hxh000

Mathematical and computational models of incompressible materials subject to shear

J. H. ADLER¹, L. DORFMANN², D. HAN^{1*}, S. MACLACHLAN¹, AND C. PAETSCH²

¹ Department of Mathematics, Tufts University, Medford, MA 02155

² Department of Civil and Environmental Engineering, Tufts University, Medford, MA 02155

*503 Boston Ave., Medford, MA 02155. E-mail: dong.han@tufts.edu

[March 12th, 2014]

Numerical modeling of incompressible nonlinear elastic materials plays an increasing role in computational science and engineering, particularly in the high-fidelity simulation of rubber-like materials and many biological tissues. Our present study focuses on the treatment of the incompressibility constraint in finite-element discretizations for a cube subject to “simple shear”. We demonstrate that this test problem is not easily captured in three-dimensional mathematical and computational models, with challenges related to the incompressibility constraint that are unique to each approach. Specifically, we review the mathematical model, which presupposes the simple shear deformation and requires additional assumptions to determine the response. A computational model avoids these difficulties, but gives rise to questions regarding the mismatch between continuum and discrete representations of material incompressibility. We consider three distinct finite-element formulations to enforce (near) incompressibility, with particular attention paid to the competing goals of physical fidelity and computational efficiency. We demonstrate that some of these standard approaches fail to resolve incompressibility in a point-wise manner, despite it holding in an averaged sense. Numerical results indicate the maximum ratio of deformed to undeformed volumes grows sharply with mesh refinement; this is in contrast to the mathematical model, but occurs in a manner consistent with finite-element convergence theory.

Keywords: incompressible materials, slightly compressible materials, simple shear, mixed finite-element methods

1 Introduction

Mathematical and computational modeling of incompressible or slightly compressible materials has a long history, starting with the work of Ogden (1972a, 1976, 1978), and including many others (Arnold et al., 1984a,b; Hughes, 1977; Hughes and Malkus, 1983; Malkus and Hughes, 1978; Simo et al., 1985). Recently, the topic has returned to the literature, with a focus on developing accurate and efficient simulation tools for modeling biological tissues and rubber-like materials (Bose and Dorfmann, 2009; deBotton et al., 2013; Horgan and Murphy, 2007, 2009c, 2010, 2011; Paetsch and Dorfmann, 2013; Rashid et al., 2013). This subject combines several challenging aspects, requiring nonlinear material laws (to account for effects of large strain), geometric nonlinearities (to account for large deformations), and accurate modeling of incompressibility, or slight compressibility, of the underlying materials, all for complex three-dimensional geometries. This paper explores the numerical simulation of incompressible and slightly compressible, nonlinear, hyperelastic materials in three dimensions, using the example of a cube of neo-Hookean material subject to simple shear. This allows us to focus on the interplay of the mathematical and computational models in the simplest possible setting.

The nonlinear theory of elasticity was used by Rivlin (1948) to analyze a cuboidal block of either compressible or incompressible material subject to simple shear. He demonstrated that for large elastic deformations, the state of simple shear cannot be supported by tangential surface traction, as in the case of small deformation using the linear theory of elasticity. In particular, Rivlin (1948) showed that for an incompressible material, the magnitude of the surface tractions is not determined uniquely since a hydrostatic pressure can always be added to the system without changing the state of deformation. The recent publication by Gent et al. (2007) and the increased use of mathematical and computational models to analyze the behavior of incompressible and highly deformable biological materials has created renewed interest in this topic. For example, Horgan and Murphy (2010) derived alternative expressions of the normal stress components in an incompressible cube of neo-Hookean material and its slightly compressible counterpart subject to simple shear. In the context of biological materials, Mihai and Goriely (2011) analyzed the orientation of the Poynting effect when a biopolymer gel is sheared between two plates. Furthermore, Rashid et al. (2013) used simple shear to characterize the mechanical properties of brain tissue, and Horgan and Murphy (2011) used it to analyze materials with preferred directions.

In the context of computational modeling, finite-element simulation of nonlinear materials is, itself, a well-studied subject, covered in numerous texts and research papers; see, for example, Belytschko et al. (2000), Bonet and Wood (2008), or Crisfield (1991). However, material incompressibility deserves particular attention. Challenges include the fundamental choice between the use of specialized slightly compressible or fully incompressible numerical approaches, where a poor choice can easily lead to slowly converging linearization strategies, or to non-physical solutions, due to the effects of “locking” or unsatisfied inf-sup stability conditions. Effectively addressing these challenges is made even more difficult by the lack of well-developed test problems in this area, where the mathematical and computational aspects of the solution process are well-understood. While this paper focuses on the finite-element approach, we also note that similar challenges arise in modeling with other approaches, such as meshless methods (Chi et al., 2014; Wu et al., 2012).

The main focus of this paper is, then, to utilize simple shear deformation as a test problem to understand treatment of the incompressibility constraint in a computational framework. For two (unrelated) mixed finite-element models, we see strong divergence in the maximum ratio of deformed to undeformed volumes across a series of three-dimensional meshes. Thus, while the (physical) incompressibility constraint is enforced in a weak (or averaged) sense by these models, pointwise measures of the volume change may show strong non-physical effects. This is, nonetheless, consistent with standard finite-element convergence theory, in that the growth in volume ratio occurs over correspondingly smaller volumes of the undeformed cube. Computational results can deviate from what is intuitively expected from the physical and mathematical descriptions. Thus, in addition to the results presented regarding the volumetric change, we address issues related to the deviating results obtained by the two approaches. We note that the disconnects between the mathematical and computational models of simple shear have been studied recently in two dimensions (Auricchio et al., 2013). However, there are significant effects in three-dimensional shear deformation that are not necessarily present in two dimensions, where plane-strain or plane-stress considerations may yield varying results.

The remainder of this paper is organized as follows. Section 2 details the basic equations, describing the incompressible and slightly compressible formulations for nonlinear deformations. Section 3 describes the prototypical simple shear problem and reviews solution techniques. A discussion of computational models is then given in Section 4. Next, simple analytical results demonstrating the misfit between the models considered are given in Section 5. Finally, more detailed numerical results are presented in Section 6, with an accompanying discussion in Section 7.

2 Basic equations

In the following, we provide an overview of the main concepts of continuum mechanics that are necessary to describe the test problem. Note that, in this paper, we focus on fully incompressible nonlinear elastic materials and on the slightly compressible (also called almost incompressible or nearly incompressible) counterpart. The theory of slightly compressible materials, originally developed for rubber-like solids, is given by Ogden (1972a, 1976, 1978). Different formulations of the volumetric part of the strain energy function have recently been proposed by Horgan and Murphy (2007, 2009a,b,c). For a detailed background on nonlinear elasticity, we refer to the books by Ciarlet (1988); Holzapfel (2001); and by Ogden (1997); the collection of articles in Fu and Ogden (2001); and Section 3 of Dorfmann and Ogden (2014).

2.1 Kinematics

To describe the deformation, we denote the stress-free reference configuration of the solid by \mathcal{B}_r and identify a generic material point by its position vector, \mathbf{X} , relative to an arbitrarily chosen origin. Application of mechanical forces deforms the body, so that the point, \mathbf{X} , occupies the new position, $\mathbf{x} = \boldsymbol{\chi}(\mathbf{X})$, in the deformed configuration, \mathcal{B} . The vector field, $\boldsymbol{\chi}$, describes the deformation of the body and assigns to each point, \mathbf{X} , a unique position, \mathbf{x} in \mathcal{B} , and vice-versa. In other words, the deformation function, $\boldsymbol{\chi}$, is a one-to-one mapping with suitable regularity properties.

The deformation gradient tensor, \mathbf{F} , relative to \mathcal{B}_r , is defined by

$$\mathbf{F} = \text{Grad } \boldsymbol{\chi}, \quad (2.1)$$

where Grad is the gradient operator with respect to \mathbf{X} . The Cartesian components are $F_{i\alpha} = \partial x_i / \partial X_\alpha$, where x_i and X_α are the components of \mathbf{x} and \mathbf{X} , respectively, with $i, \alpha \in \{1, 2, 3\}$. Roman indices are associated with \mathcal{B} and Greek indices with \mathcal{B}_r . We also adopt the standard notation, J , to denote the volume ratio given by

$$J = \det \mathbf{F} = \frac{dv}{dV} > 0, \quad (2.2)$$

where v denotes the deformed volume and V denotes the undeformed volume. For incompressible materials or volume preserving (isochoric) deformations, we have $J = 1$ pointwise in \mathcal{B}_r .

The deformation gradient can be decomposed pointwise according to the unique polar decomposition,

$$\mathbf{F} = \mathbf{R}\mathbf{U} = \mathbf{V}\mathbf{R}, \quad (2.3)$$

where \mathbf{R} is a proper orthogonal tensor and \mathbf{U} and \mathbf{V} are positive definite and symmetric, and are called the right and left stretch tensors, respectively. These can be expressed in spectral form. For \mathbf{U} , the spectral decomposition is

$$\mathbf{U} = \sum_{i=1}^3 \lambda_i \mathbf{u}^{(i)} \otimes \mathbf{u}^{(i)}, \quad (2.4)$$

where the principal stretches $\lambda_i > 0$, $i \in \{1, 2, 3\}$, are the eigenvalues of \mathbf{U} , $\mathbf{u}^{(i)}$ are the (unit) eigenvectors of \mathbf{U} , and \otimes denotes the tensor product. Using the polar decomposition (2.3), we define

$$\mathbf{C} = \mathbf{F}^T \mathbf{F} = \mathbf{U}^2, \quad \mathbf{B} = \mathbf{F} \mathbf{F}^T = \mathbf{V}^2, \quad (2.5)$$

which denote the right and left Cauchy-Green deformation tensors, respectively. According to the theory of invariants (Spencer, 1971), there exist three principal invariants for \mathbf{C} , or equivalently \mathbf{B} , defined by

$$I_1 = \text{tr} \mathbf{C}, \quad I_2 = \frac{1}{2} [(\text{tr} \mathbf{C})^2 - \text{tr}(\mathbf{C}^2)], \quad I_3 = \det \mathbf{C} = J^2, \quad (2.6)$$

where tr is the trace of a second-order tensor. Alternatively, in terms of principal stretches, the invariants, I_1, I_2, I_3 , are expressed as

$$I_1 = \lambda_1^2 + \lambda_2^2 + \lambda_3^2, \quad I_2 = \lambda_1^2 \lambda_2^2 + \lambda_2^2 \lambda_3^2 + \lambda_3^2 \lambda_1^2, \quad I_3 = \lambda_1^2 \lambda_2^2 \lambda_3^2. \quad (2.7)$$

2.2 Incompressible materials

The theory of hyperelasticity characterizes the elastic response of a body by a strain-energy density function, W , defined per unit volume in the reference configuration \mathcal{B}_r . For homogeneous materials, W depends only on the deformation gradient \mathbf{F} , and is written $W = W(\mathbf{F})$. Recall that $W(\mathbf{F})$ represents the work, per unit reference volume, done by the stress in deforming the material from \mathcal{B}_r to \mathcal{B} . Later, for the computational model, we introduce the total strain energy, π , which is defined as the volume integral of W , $\pi = \int_{\mathcal{B}_r} W(\mathbf{F}) dV$.

In this section, attention is restricted to incompressible materials, subject to the constraint $J = 1$. From the energy balance equation, we find that the nominal stress tensor, \mathbf{S} , and the symmetric Cauchy stress tensor, $\boldsymbol{\sigma}$, are given, respectively, by

$$\mathbf{S} = \frac{\partial W}{\partial \mathbf{F}} - p \mathbf{F}^{-1}, \quad \boldsymbol{\sigma} = \mathbf{F} \frac{\partial W}{\partial \mathbf{F}} - p \mathbf{I}, \quad (2.8)$$

where p is the Lagrange multiplier (Ogden, 1997). Equation (2.8) shows that for an incompressible material, the Cauchy stress, $\boldsymbol{\sigma}$, and the nominal stress, \mathbf{S} , are related by $\boldsymbol{\sigma} = \mathbf{F} \mathbf{S}$.

The strain energy is not affected by a rigid body rotation. Therefore, for an isotropic material the stored energy can be expressed as a symmetric function of λ_1, λ_2 , and λ_3 or, alternatively, in terms of the invariants in (2.7). Many different strain-energy density functions are available to model the incompressible behavior of rubberlike solids, and we refer to deBotton et al. (2013) and Ogden (1972b) for an overview and applications. In this paper, we restrict attention to the nonlinear prototype model that is known as the incompressible neo-Hookean material, and commentary on the implication of alternate constitutive forms is provided in Section 6. The strain-energy density function has the form

$$W = \frac{1}{2} \mu (I_1 - 3), \quad (2.9)$$

where $\mu (> 0)$ is a material constant referred to as the shear modulus of the material in the reference configuration. Then, the associated nominal and Cauchy stresses (2.8) are given by

$$\mathbf{S} = \mu \mathbf{F}^T - p \mathbf{F}^{-1}, \quad \boldsymbol{\sigma} = \mu \mathbf{B} - p \mathbf{I}, \quad (2.10)$$

respectively. Assuming incompressibility and using a simple form of the strain-energy density function, it is possible to obtain explicit analytical solutions of boundary-value problems involving simple geometries and boundary conditions, see, for example, Ogden (1997). In Section 3, we note that this is only possible in the context of simple shear with added boundary conditions or forces.

2.3 Slightly compressible materials

In this section, we define the isochoric-volumetric decomposition of the relevant kinematic measures for slightly compressible materials, i.e. $J \neq 1$. Following the developments given by Ogden (1976, 1978), we adopt the multiplicative decomposition of the total deformation into volumetric and isochoric parts expressed by

$$\mathbf{F} = (J^{1/3})\bar{\mathbf{F}}, \quad (2.11)$$

where $\bar{\mathbf{F}}$ is the isochoric portion of the deformation with $\det \bar{\mathbf{F}} = 1$. The isochoric right and left Cauchy-Green tensors are, respectively, given by

$$\bar{\mathbf{C}} = \bar{\mathbf{F}}^T \bar{\mathbf{F}}, \quad \bar{\mathbf{B}} = \bar{\mathbf{F}} \bar{\mathbf{F}}^T, \quad (2.12)$$

with the principle invariants of $\bar{\mathbf{C}}$ (or equivalently $\bar{\mathbf{B}}$) written

$$\bar{I}_1 = \text{tr} \bar{\mathbf{C}}, \quad \bar{I}_2 = \frac{1}{2} [(\text{tr} \bar{\mathbf{C}})^2 - \text{tr} (\bar{\mathbf{C}}^2)], \quad \bar{I}_3 \equiv 1. \quad (2.13)$$

Alternatively, the invariants \bar{I}_1 and \bar{I}_2 can be expressed in terms of the modified stretches in the form

$$\bar{I}_1 = \bar{\lambda}_1^2 + \bar{\lambda}_2^2 + \bar{\lambda}_3^2, \quad \bar{I}_2 = \bar{\lambda}_1^{-2} + \bar{\lambda}_2^{-2} + \bar{\lambda}_3^{-2}, \quad \text{with} \quad \bar{\lambda}_1 \bar{\lambda}_2 \bar{\lambda}_3 = 1, \quad (2.14)$$

where $\bar{\lambda}_i = \lambda_i J^{-1/3}$, $i \in \{1, 2, 3\}$.

Many different isotropic strain-energy density functions have been proposed in the literature to model slightly compressible materials, see Horgan and Murphy (2007, 2009a,b,c), Destrade et al. (2012a) and Ogden (1972a) for details. Specifically, the model introduced by Ogden (1972a) is of the form

$$W_c = \bar{W}(\lambda_1, \lambda_2, \lambda_3) + F(J), \quad (2.15)$$

where W_c denotes the strain-energy density function of a compressible material and \bar{W} is a symmetric function of the principal stretches.

When the finite-element method is used to solve the equations for specified geometry and boundary conditions, the strain-energy density function for slightly compressible materials is most frequently given in the form

$$W_c = \bar{W}(\bar{I}_1, \bar{I}_2) + F(J), \quad (2.16)$$

where $\bar{W}(\bar{I}_1, \bar{I}_2)$ is the volume-preserving contribution and $F(J)$ is the volumetric portion. Ogden (1976) provides an alternative formulation in terms of the modified principal stretches, $\bar{\lambda}_1$, $\bar{\lambda}_2$, and $\bar{\lambda}_3$, given by

$$W_c = \bar{W}(\bar{\lambda}_1, \bar{\lambda}_2, \bar{\lambda}_3) + F(J), \quad (2.17)$$

where \bar{W} is a symmetric function of the modified principal stretches and again accounts for the volume-preserving part of the deformation. To ensure that Equations (2.15) - (2.17) reduce to the fully incompressible case, it is required that $F(1) = 0$. The corresponding nominal and Cauchy stresses are given, respectively, by

$$\mathbf{S} = \frac{\partial W_c}{\partial \mathbf{F}}, \quad \boldsymbol{\sigma} = J^{-1} \mathbf{F} \frac{\partial W_c}{\partial \mathbf{F}}, \quad \mathbf{S} = J \mathbf{F}^{-1} \boldsymbol{\sigma}. \quad (2.18)$$

Following Bose and Dorfmann (2009), Paetsch and Dorfmann (2013), the nominal stress is calculated by substituting expression (2.16) into \mathbf{S} in the first equation of (2.18),

$$\mathbf{S} = \frac{\partial \bar{W}}{\partial \mathbf{F}} + \frac{\partial F}{\partial \mathbf{F}} = \bar{\mathbf{S}} + \mathbf{S}_{\text{vol}}, \quad (2.19)$$

where the first term on the right-hand side represents the isochoric (or deviatoric) contribution, denoted by $\bar{\mathbf{S}}$, and the second term is the volumetric (or hydrostatic) part, denoted by \mathbf{S}_{vol} . Evaluation of equation (2.19) requires the derivatives of the isochoric strain invariants with respect to \mathbf{F} , which can be found in the aforementioned references.

For a slightly compressible neo-Hookean model, the analogue of the incompressible strain-energy density function given in (2.9) is

$$W_c = \frac{1}{2}\mu(\bar{I}_1 - 3) + \frac{\kappa}{2}(J - 1)^2 = \frac{1}{2}\mu(\bar{\lambda}_1 + \bar{\lambda}_2 + \bar{\lambda}_3 - 3) + \frac{\kappa}{2}(J - 1)^2, \quad (2.20)$$

where we note that the volumetric penalty function takes the form $F(J) = \frac{\kappa}{2}(J - 1)^2$. Here, κ is defined as the bulk modulus of the system and represents a penalty parameter in the energy functional. Note, there exist many possible forms of $F(J)$, subject to some restrictions, see Merodio and Ogden (2003) and Merodio and Neff (2006), for example. The interested reader can find alternate expressions of the volumetric elastic response function in the work of Ogden (1972a), Ehlers and Eipper (1998), Peng and Chang (1997), and the references within.

From Eq. (2.19) and the connection (2.18)₃, we find the total nominal stress is

$$\mathbf{S} = \mu J^{-1/3} \left(\bar{\mathbf{F}}^T - \frac{1}{3}\bar{I}_1 \bar{\mathbf{F}}^{-1} \right) + \kappa J(J - 1)\mathbf{F}^{-1}, \quad (2.21)$$

while the total Cauchy stress is obtained from the connection

$$\boldsymbol{\sigma} = \mu J^{-1} \text{dev}(\bar{\mathbf{B}}) + \kappa(J - 1)\mathbf{I}, \quad (2.22)$$

where (2.22) is written more concisely by introducing the deviatoric operator defined as $\text{dev}(\mathbf{A}) = \mathbb{P} : \mathbf{A}$. The fourth-order projection tensor, \mathbb{P} , has components $\mathbb{P}_{ijkl} = \delta_{ik}\delta_{jl} - (1/3)\delta_{ij}\delta_{kl}$ and \mathbf{A} is a second-order symmetric tensor. The component form of $\mathbb{P} : \mathbf{A}$ is $\mathbb{P}_{ijkl}A_{kl}$.

3 Mathematical model

3.1 Deformation for simple shear

In this section, we consider the problem involving a homogeneous deformation, known as simple shear. The mathematical problem of simple shear for nonlinear elastic materials was first considered by Rivlin (1948) and various aspects evaluated subsequently in the monographs by Truesdell and Noll (1965) and by Ogden (1997). Motivated by the publication by Gent et al. (2007), the mathematical treatment of simple shear has attracted renewed interest in recent years. For isotropic materials we list, for example, the papers by Horgan and Murphy (2010), Destrade et al. (2012a,b), Mihai and Goriely (2011) and Rashid et al. (2013). Simple shear deformation involving fiber reinforced biological tissues is discussed by Horgan and Murphy (2011). For convenience of reference, we provide a brief summary next.

Simple shear in the X_1 -direction in the (X_1, X_3) plane with an amount of shear, γ , is defined in component form by

$$x_1 = X_1 + \gamma X_3, \quad x_2 = X_2, \quad x_3 = X_3. \quad (3.1)$$

The matrix of Cartesian components, F , of the deformation gradient tensor, \mathbf{F} , is

$$F = \begin{pmatrix} 1 & 0 & \gamma \\ 0 & 1 & 0 \\ 0 & 0 & 1 \end{pmatrix}. \quad (3.2)$$

For simple shear, the principal invariants, I_1 , I_2 , and I_3 , defined in Equation (2.6), simplify to

$$I_1 = I_2 = 3 + \gamma^2, \quad I_3 = 1. \quad (3.3)$$

3.2 Stress response for an incompressible material

For an incompressible material, we solve for the Lagrange multiplier, defined in (2.8), in order to determine the material response, even when the deformation is given. For the case of simple shear, this is not straightforward, and there are several examples in the literature, which address this issue (Gent et al., 2007; Horgan and Murphy, 2010; Mihai and Goriely, 2011; Rivlin, 1948). Here, we provide an overview of the topic to provide context for the deviation in the numerical results from the prescribed simple shear deformation given by (3.2).

By substituting \mathbf{B} into the stress-deformation relation defined in (2.10), we find the stress components for an incompressible neo-Hookean material associated with simple shear in the form,

$$\sigma_{11} = \mu(1 + \gamma^2) - p, \quad \sigma_{22} = \sigma_{33} = \mu - p, \quad \sigma_{13} = \mu\gamma, \quad (3.4)$$

where we note that the simple shear deformation is associated with normal stress components, σ_{11} , σ_{22} , and σ_{33} , as well as with the shear stress, σ_{13} . The remaining two shear components, σ_{12} and σ_{23} , are zero everywhere for this deformation. Expressions of the stress components corresponding to a general energy-density function, $W = W(I_1, I_2)$, are given, for example, in Rivlin (1948) and Horgan and Murphy (2010). In these works, it is shown that traction boundary conditions must be applied to maintain the deformation in (3.1). Figure 1 shows that the outward unit normal, \mathbf{n} , and the unit tangent vector, \mathbf{s} , in the (X_1, X_3) plane are given, respectively, by

$$\mathbf{n} = \frac{1}{\sqrt{1 + \gamma^2}} (\mathbf{e}_1 - \gamma \mathbf{e}_3), \quad \mathbf{s} = \frac{1}{\sqrt{1 + \gamma^2}} (\gamma \mathbf{e}_1 + \mathbf{e}_3), \quad (3.5)$$

where \mathbf{e}_1 and \mathbf{e}_3 are the unit basis vectors.

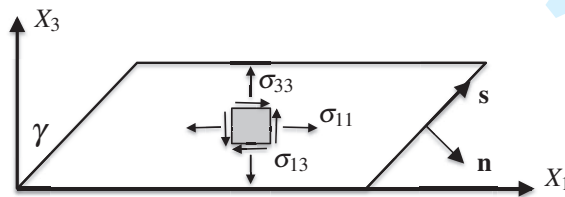


FIG. 1: Cuboidal block subject to simple shear in the (X_1, X_3) plane. The amount of shear is γ , the outward unit normal and the tangent vector on the inclined face are \mathbf{n} and \mathbf{s} , respectively. The orientations of the in-plane stress components are depicted as well.

The normal component, $N = \mathbf{t} \cdot \mathbf{n}$, and the tangential component, $S = \mathbf{t} \cdot \mathbf{s}$, of the traction vector, $\mathbf{t} = \boldsymbol{\sigma} \mathbf{n}$, on the inclined faces of the deforming body are

$$N = \sigma_{33} - \gamma S, \quad S = \frac{\sigma_{13}}{1 + \gamma^2}, \quad (3.6)$$

where the universal relation, $\sigma_{11} - \sigma_{33} = \gamma\sigma_{13}$, is used. Therefore, a normal component, N , is required to maintain the deformation in (3.1). Similarly, the traction vector on the plane, whose outward pointing unit vector is in the 2-direction, is equal to σ_{22} .

To complete the solution, the unknown Lagrange multiplier, p in (3.4), needs to be determined, which can be done in several different ways (Horgan and Murphy, 2010). Following Rivlin (1948), we consider a plane stress condition, where the surfaces defined by unit vectors in the 2-direction are traction free, i.e. $\sigma_{22} = 0$ and, therefore, $p = \mu$. From (3.4), we find

$$\sigma_{11} = \mu\gamma^2, \quad \sigma_{22} = \sigma_{33} = 0, \quad \sigma_{13} = \mu\gamma. \tag{3.7}$$

For the slightly more general Mooney-Rivlin material, $W = W(I_1, I_2)$, the stress in the 3-direction is negative (compressive) and has the form $\sigma_{33} = -2\gamma^2 \partial W / \partial I_2$.

For small deformations considered in the classical theory of elasticity, simple shear deformation is generated by shear stress only. Therefore, an alternative approach is to assume that the normal component of the traction vector on the inclined faces, given by the normal component in (3.6), vanishes (Gent et al., 2007; Horgan and Murphy, 2010; Rivlin, 1948). The value of the unknown Lagrange multiplier, p , is then given by

$$p = \frac{\mu}{1 + \gamma^2}, \tag{3.8}$$

and, using (3.4), we find the normal stress components,

$$\sigma_{11} = \frac{\mu\gamma^2(2 + \gamma^2)}{1 + \gamma^2}, \quad \sigma_{22} = \sigma_{33} = \frac{\mu\gamma^2}{1 + \gamma^2}, \tag{3.9}$$

which clearly differ from (3.7). The shear stress is not affected and is still given by $\sigma_{13} = \mu\gamma$. The sign of the normal components is positive, indicating tensile stresses. For the plane stress condition, using a Mooney-Rivlin material, σ_{33} is negative, indicating a compressive stress. These ambiguities are elaborated in great detail by Horgan and Murphy (2010), who also derived the corresponding expressions in terms of principal stretches.

For the slightly compressible neo-Hookean material given in (2.20), the deformation given in (3.2) leads to a Cauchy stress, from (2.18) or (2.22), of

$$\sigma_{11} = \frac{2}{3}\mu\gamma^2, \quad \sigma_{22} = \sigma_{33} = -\frac{1}{3}\mu\gamma^2, \quad \sigma_{13} = \mu\gamma. \tag{3.10}$$

The normal and tangential components of the traction vector on the inclined surfaces are given by $N = \boldsymbol{\sigma}\mathbf{n} \cdot \mathbf{n}$ and $S = \boldsymbol{\sigma}\mathbf{n} \cdot \mathbf{s}$. For a slightly compressible material these are given by

$$N = -\frac{\mu\gamma^2(4 + \gamma^2)}{3(1 + \gamma^2)}, \quad S = \frac{\mu\gamma}{1 + \gamma^2}, \tag{3.11}$$

where we recall that the components of the unit vectors, \mathbf{n} and \mathbf{s} , are defined by (3.5). We note that the tangential component of the traction vector defined here matches that given for the incompressible case in (3.6), but the normal components are different when $p = \mu$ is chosen, as in (3.7).

These considerations highlight the difficulty of obtaining consistent results for this commonly considered test problem. It is therefore no surprise that in the following section, by applying boundary conditions consistent with simple shear at two surfaces of a cube, our numerical results do not reproduce the homogeneous deformation considered in the mathematical model, except for a few special cases.

4 Computational models

Since analytical approaches for minimizing the total strain energy are only applicable in special cases, we next discuss commonly used computational approaches for approximately minimizing that energy. We focus on finite-element formulations and consider how their properties, including enforcement of boundary conditions, correspond to the conditions needed for a simple shear deformation.

Computational methods for modeling incompressible deformation are naturally divided into those based on the fully incompressible approach described in Section 2.2, those based on the slightly compressible formulation discussed in Section 2.3, and those that use a “hybrid” formulation, which is more robust than the standard formulation in the slightly compressible case; see, for example, Bonet and Wood (2008), Belytschko et al. (2000) or Crisfield (1991). In all three cases, the total strain energy is minimized by solving the (nonlinear) first-order optimality conditions, such that the total strain energy is stationary at its minimum. To solve these nonlinear equations, Newton’s method (or some variant) is applied to the first-order optimality conditions, yielding a series of linear systems to be solved for the Newton iterates. These systems are discretized using the finite-element method (often referred to as the principle of virtual work) (Belytschko et al., 2000; Boffi et al., 2013), although we note that first-order optimality conditions can also be discretized before they are linearized.

For the neo-Hookean materials considered here, the computational models are based on minimizing the integrated strain energy density, referred to as the total strain energy. For the incompressible model, we augment the strain-energy density function in (2.9) with a Lagrange multiplier to enforce incompressibility, and integrate over the reference configuration,

$$\pi_{\text{FI}} = \int_{\mathcal{B}_r} \frac{\mu}{2} (I_1 - 3) + p(J - 1) dV, \quad (4.1)$$

where the subscript FI indicates this is the fully incompressible formulation. Since the Lagrange multiplier is used here to enforce $J = 1$, a nearly equivalent formulation is to consider

$$\pi_{\text{FI}} = \int_{\mathcal{B}_r} \frac{\mu}{2} (\bar{I}_1 - 3) + p(J - 1) dV, \quad (4.2)$$

where the standard invariant, I_1 , is replaced by \bar{I}_1 defined in (2.13). In the computational results in Section 6, we use (4.2) to drive the minimization, ensuring a true separation into volumetric and isochoric work, although analytical results in Section 5 rely on the simpler form in (4.1). For the slightly compressible case, denoted by a subscript SC, we use the strain-energy density function from (2.20), giving

$$\pi_{\text{SC}} = \int_{\mathcal{B}_r} \frac{\mu}{2} (\bar{I}_1 - 3) + \frac{\kappa}{2} (J - 1)^2 dV. \quad (4.3)$$

For comparison, in Section 6, we also include results for a “hybrid” formulation for slightly compressible materials, as implemented in Abaqus FEA (Dassault Systèmes Simulia, 2009). In all cases, the strain-energy functional is rewritten in terms of the displacement vector, \mathbf{u} (taking $\boldsymbol{\chi}(\mathbf{X}) = \mathbf{X} + \mathbf{u}(\mathbf{X})$), leading to a nonlinear minimization problem.

The equilibrium equations are then obtained by doing a variation of the appropriate strain-energy functional with respect to the dependent variables, \mathbf{u} (and p in the incompressible and hybrid cases), and setting the derivatives to zero. The resulting Euler-Lagrange equations are nonlinear, and a linearization is performed to yield a solution scheme, iteratively taking $\mathbf{u} \rightarrow \mathbf{u} + \dot{\mathbf{u}}$ and $p \rightarrow p + \dot{p}$ (if necessary). In this simple case, we consider a standard Newton step on the equilibrium equations. Thus, for the slightly

compressible case, we obtain a linear equation,

$$\left(\overline{\delta_u \pi_{SC}(\mathbf{u}_k)} \right)_{\dot{\mathbf{u}}} \dot{\mathbf{u}} = -\delta_u \pi_{SC}(\mathbf{u}_k), \quad (4.4)$$

and for the fully incompressible or hybrid cases, we obtain

$$\begin{pmatrix} \left(\overline{\delta_u \pi_{FI}(\mathbf{u}_k, p_k)} \right)_{\dot{\mathbf{u}}} & \left(\overline{\delta_u \pi_{FI}(\mathbf{u}_k, p_k)} \right)_{\dot{p}} \\ \left(\overline{\delta_p \pi_{FI}(\mathbf{u}_k, p_k)} \right)_{\dot{\mathbf{u}}} & \left(\overline{\delta_p \pi_{FI}(\mathbf{u}_k, p_k)} \right)_{\dot{p}} \end{pmatrix} \begin{pmatrix} \dot{\mathbf{u}} \\ \dot{p} \end{pmatrix} = \begin{pmatrix} -\delta_u \pi_{FI}(\mathbf{u}_k, p_k) \\ -\delta_p \pi_{FI}(\mathbf{u}_k, p_k) \end{pmatrix}, \quad (4.5)$$

where the dot notation indicates a linearization about some previous iteration, (\mathbf{u}_k, p_k) . Note that, in the fully incompressible case, the lower right block in system (4.5) is generally zero, due to the fact that the fully incompressible energy is linear in p . However, in certain mixed-form finite-element methods, a stabilization term is added in this block to guarantee inf-sup stability. The five other terms (including the right-hand sides) in the above Hessian system, (4.5), and the terms in (4.4), can all be computed explicitly in terms of known quantities, coming from the domain, the invariants of the system, and the deformation at the previous linearization step. Thus, the nonlinear solution algorithm, specifically for the fully incompressible case, is as follows:

Algorithm 1: Variation and linearization steps for incompressible nonlinear elasticity.

0. Set $k = 0$, $\mathbf{u}_0 = 0$, and $p_0 = 0$.

while *Nonlinear Iterations Not Converged* **do**

1. Compute $\delta_u \pi_{FI}(\mathbf{u}_k, p_k)$, $\delta_p \pi_{FI}(\mathbf{u}_k, p_k)$, $\left(\overline{\delta_u \pi_{FI}(\mathbf{u}_k, p_k)} \right)_{\dot{\mathbf{u}}}$, $\left(\overline{\delta_u \pi_{FI}(\mathbf{u}_k, p_k)} \right)_{\dot{p}}$, $\left(\overline{\delta_p \pi_{FI}(\mathbf{u}_k, p_k)} \right)_{\dot{\mathbf{u}}}$, $\left(\overline{\delta_p \pi_{FI}(\mathbf{u}_k, p_k)} \right)_{\dot{p}}$
2. Solve system (4.5) for $\dot{\mathbf{u}}$ and \dot{p} .
3. $\mathbf{u}_{k+1} = \mathbf{u}_k + \dot{\mathbf{u}}$, $p_{k+1} = p_k + \dot{p}$, $k = k + 1$.

end

4.1 Finite-element spaces

From the linearization process, we next need to choose finite-element spaces for \mathbf{u} and p , choosing appropriate sets of basis functions for their discrete representation on the computational mesh. For the standard slightly compressible formulation, the linearization and discretization process is somewhat straightforward, with a wide array of acceptable finite-element spaces. In this setting, there is no auxiliary variable, p , and, so, the Hessian has only one block in contrast to the fully incompressible case given in (4.5). Thus, the Hessian of the slightly compressible model, (4.4), remains invertible for all linearizations in the Newton iteration using standard choices of the finite-element spaces, including typical piecewise-polynomial spaces defined on tetrahedral and hexahedral meshes. As a result, the important criterion in the choice of the discretization space is the trade-off of potential accuracy versus the computational cost of solving the resulting linear systems (Braess, 2007). While this computational cost is often equated with, simply, the size of the resulting linear system, a more subtle calculus arises when considering the construction of optimal preconditioning strategies for these systems. Since we only

consider direct solves of the resulting linearized systems, issues of robust and scalable preconditioners do not arise directly in our numerical results.

For this paper, we assume a hexahedral mesh, \mathcal{T}_h , of the domain, \mathcal{B}_r , with uniform mesh spacing, h . We denote by $\mathcal{P}_k(T)$ the space of polynomial functions of degree at most k defined on a generic element, $T \in \mathcal{T}_h$. Then, the discrete finite-element spaces considered are the piecewise-polynomial spaces of order k with enforced continuity across element boundaries,

$$\mathbf{Q}k = \{u \in H^1(\mathcal{B}_r) \cap C^0(\mathcal{B}_r) : u|_T \in \mathcal{P}_k(T)^3 \quad \forall T \in \mathcal{T}_h\},$$

and the piecewise-polynomial spaces of order k that are allowed to be discontinuous across element boundaries,

$$\mathbf{P}k = \{u \in L_2(\mathcal{B}_r) : u|_T \in \mathcal{P}_k(T)^3 \quad \forall T \in \mathcal{T}_h\}.$$

Here, $L_2(\mathcal{B}_r)$ refers to the space of square-integrable functions on \mathcal{B}_r and $H^1(\mathcal{B}_r) = \{u \in L_2(\mathcal{B}_r) : \nabla u \in L_2(\mathcal{B}_r)\}$ is the first-order Sobolev space. In Section 6, we present results for the Q2 finite-element discretization of the standard slightly compressible formulation, using triquadratic basis functions for each component of the displacement on each element. Since there is no ambiguity in their use, we do not distinguish in notation between the scalar finite-element spaces defined above and their vector counterparts used for displacements.

For the Q2 finite-element space considered here, assuming sufficient regularity of the domain and solution, classical error bounds are obtained for the discrete solution of the displacement, \mathbf{u}_h , compared to the continuum solution, \mathbf{u} :

$$\|\mathbf{u} - \mathbf{u}_h\|_0 \leq C(\mu, \kappa) h^3 |\mathbf{u}|_3,$$

where the norm on the left is the usual L_2 norm, and that on the right is the usual semi-norm of the Sobolev space H^3 ; with additional regularity and increasing polynomial order, k , the error bound scales as h^{k+1} . Therefore, using higher-order spaces and more refined meshes should reduce the discretization error. However, since the constant, C , depends on the material parameters, μ , and κ , we are not guaranteed a uniform bound as $\kappa/\mu \rightarrow \infty$, the case of interest.

Since such classical error bounds do apply, the primary concern in the choice of finite-element bases for the slightly compressible formulation is one of avoiding the well-known problem of ‘‘volumetric locking’’, where non-physical results may be given and convergence of the nonlinear iteration suffers. The phenomenon of volumetric locking occurs in the slightly compressible case when the bulk modulus, κ , (acting as a penalty parameter) becomes large in comparison to μ , enforcing the incompressibility constraint too strongly for the solution to remain physically meaningful. In this instance, deviations in the volumetric constraint, $J = 1$, dominate the energy at the scale where numerical errors in the constraint dominate the solution. As a result, it is difficult to computationally minimize the energy in a way that is consistent with the physical problem. Mathematically, this is associated with an ‘‘over-constraining’’ of the solution within the finite-element space.

Several solutions have been presented to reduce the effects of locking in the slightly compressible case. A straight-forward approach is to use higher-order finite-element methods or over-resolved meshes in order to lessen the effects of the constraint. More commonly, reduced integration techniques are used (Belytschko et al., 1984; Hughes, 1977, 1980; Hughes and Malkus, 1983; Malkus and Hughes, 1978), replacing the exact integral in (4.3) with a suitable approximation. While these methods reduce the effects of volumetric locking, the resulting linear systems may be more difficult to solve, thus increasing the overall computational cost of the method. These approaches can still lead to difficulties when $\kappa \gg \mu$, only delaying the onset of such problems for large κ . In some cases, however, reduced integration

approaches are equivalent to the use of the fully incompressible strain energy, such as for suitably chosen discontinuous approximations of the Lagrange multiplier (Malkus and Hughes, 1978).

An alternative approach is to augment the variational formulation with additional variables in a two-field or three-field formulation (Belytschko et al., 2000; Doghri, 2000; Simo and Taylor, 1991; Simo et al., 1985). In Section 6, we compare the slightly compressible and fully incompressible results with the three-field “hybrid” formulation implemented in Abaqus FEA (Dassault Systèmes Simulia, 2009), in which the displacement degrees of freedom are augmented by an independent hydrostatic pressure variable, which is coupled to the physical hydrostatic pressure via a Lagrange multiplier. While we refer to this as a “three-field” formulation, the Lagrange multiplier is eliminated algebraically through a symmetry argument and the introduction of an *instantaneous* bulk modulus, leaving just the displacement and hydrostatic pressure variables as unknowns in the final system.

While the complete formulation of this “hybrid” approach is too involved to readily summarize here, two salient points are important. First, the approach includes the slightly compressible material law, as given in (2.16) (see (2.20) for the Neo-Hookean case), and not the incompressible law in (2.9); as a result, the bulk modulus remains as a penalty parameter. Second, the augmentation is done in a way so that the Hessian system (analogous to that given in (4.5) for the fully incompressible case) is always invertible, with a negative-definite second variation with respect to p . While this guarantees that no discrete stability condition (inf-sup or Ladyzhenskaya-Babuska-Brezzi (LBB) condition (Boffi et al., 2013; Braess, 2007; Brenner and Scott, 2002)) needs to be satisfied, typical practice is to take the approximation of hydrostatic pressure from a lower-dimensional space, such as using Q2 (triquadratic) basis functions for displacements and Q1 (trilinear) basis functions for the hydrostatic pressure. For the detailed formulation, the interested reader is referred to the Abaqus FEA Theory Manual (Dassault Systèmes Simulia, 2009).

For the fully incompressible strain energy in (4.2), using mixed finite-elements, as in the “hybrid” case, is also a natural choice, separately approximating the displacements and the Lagrange multiplier. This eliminates the issue of volumetric locking from the standard slightly compressible formulation, as in the hybrid case discussed above. However, the fully incompressible formulation does raise problems with stability of the discretization and invertibility of the Hessian in (4.5).

For incompressible linear elasticity, such questions are well-understood. In order to ensure stability (equivalently, invertibility of (4.5)), an inf-sup or LBB condition must be satisfied, constraining the choices of discretization spaces for the two variables (Adams and Cockburn, 2005; Arnold et al., 1984a, 2007; Arnold and Winther, 2002; Boffi et al., 2013; Brenner and Scott, 2002). This condition enforces *weak coercivity*, ensuring well-posedness of the formulation. For linear elasticity, pairs of spaces that satisfy such (problem-dependent) conditions are well-known, such as the Taylor-Hood (Q2Q1) elements, which (for hexahedral meshes) combine Q2 (triquadratic) approximations for displacements with Q1 (trilinear) approximations for the Lagrange multiplier, or the slightly lower-order approximation, Q2P0, with Q2 displacements and a P0 (piecewise-constant) Lagrange multiplier. Using equal-order elements, such as Q1 approximations for both the displacements and the Lagrange multiplier, is known to not be stable without either the addition of a non-physical (but asymptotically vanishing) stabilization term to the second variation with respect to p , akin to what appears naturally in the hybrid formulation. For the simulations in Section 6, we use a standard stabilization approach for Q1Q1 elements in the Stokes’ system (Dohrmann and Bochev, 2004; Elman et al., 2005). In this approach, the lower-right block of (4.5) is replaced by a “pressure-projection” operator,

$$\left(\overline{\delta_p \pi_{FI}(\mathbf{u}_k, p_k)} \right)_p = -\langle \delta_p - \Pi_0 \delta_p, \dot{p} - \Pi_0 \dot{p} \rangle, \quad (4.6)$$

where Π_0 is the projection from Q1 onto P0 and $\langle \cdot, \cdot \rangle$ indicates an $L_2(\Omega)$ inner product. Other stabilization methods include augmenting the displacement space with bubble functions, as is done in MINI elements (Arnold et al., 1984b).

For the nonlinear problems at hand here, similar theoretical results are not known, but empirical evidence suggests such spaces are appropriate (cf. Rossi et al. (2012); Ruiz-Baier et al. (2013)). The numerical results that follow use these finite-element spaces, and we encounter no numerical difficulties suggesting problems with stability. Additionally, error analysis for these mixed formulations is complicated by their reliance on inf-sup stability bounds. Nonetheless, we can gain insight from bounds for cases where stability results are known, such as for the Stokes' equations and linear elasticity (Boffi et al., 2013; Brenner and Scott, 2002; Elman et al., 2005). For the Stokes' equations, standard error bounds (assuming sufficient regularity on the domain, mesh, and solution) (Elman et al., 2005) are:

$$\text{Q2Q1: } \|\nabla(\mathbf{u} - \mathbf{u}_h)\|_0 + \|p - p_h\|_0 \leq C_1 h^2 (|\mathbf{u}|_3 + |p|_2),$$

$$\text{Q2P0: } \|\nabla(\mathbf{u} - \mathbf{u}_h)\|_0 + \|p - p_h\|_0 \leq C_2 h (|\mathbf{u}|_3 + |p|_1),$$

$$\text{Q1Q1: } \|\nabla(\mathbf{u} - \mathbf{u}_h)\|_0 + \|p - p_h\|_0 \leq C_3 h (|\mathbf{u}|_2 + |p|_1),$$

where the standard Sobolev semi-norms of orders 1, 2, and 3 appear on the right-hand sides, and C_1 , C_2 , and C_3 are arbitrary constants. Assuming similar bounds hold for the nonlinear problem considered here, this would guarantee convergence of both the computed displacements, \mathbf{u}_h , and Lagrange multiplier, p_h , to their continuum values, \mathbf{u} and p , with grid refinement. We note, however, that this offers no guarantee of uniform convergence of $J_h = \det(I + \text{Grad} \mathbf{u}_h)$ to one. In fact, results in Section 6 show divergence in the maximum value of J_h as $h \rightarrow 0$; based on these error estimates, we can only guarantee that increasing values of J_h must be confined to smaller regions as $h \rightarrow 0$, as observed, for example, in Figure 8. Finally, we provide a summary of the finite-element spaces considered in Table 1.

Table 1: Summary of finite-element spaces.

Method	Software	Variables	Approximation	Eqn. Form
Q2	Abaqus FEA	\mathbf{u}	<i>Slightly Compressible</i> triquadratic	(4.3)
Q2A	Abaqus FEA	\mathbf{u}, p	<i>Hybrid</i> triquadratic, trilinear	(Dassault Systèmes Simulia, 2009)
Q1Q1	deal.II	\mathbf{u}, p	<i>Fully Incompressible</i> trilinear, trilinear	(4.2) & (4.6)
Q2P0	deal.II	\mathbf{u}, p	triquadratic, piecewise-constant	(4.2)
Q2Q1	deal.II	\mathbf{u}, p	triquadratic, trilinear	(4.2)

4.2 Boundary conditions

In contrast to the discussions in Sections 3.1 and 3.2, the computational models apply boundary conditions specifying the displacement or the normal component of the referential displacement gradient. For the simple shear example treated here, the boundary conditions applied on the top and bottom faces

enforce the deformation given in (3.1). Specifically, the boundary conditions on the unit cube, $[0, 1]^3$, include fixing all three components of displacement to be zero along the face $X_3 = 0$ and fixing the sheared displacement to give $x_1 = X_1 + \gamma$, $x_2 = X_2$, $x_3 = X_3$ along the face $X_3 = 1$. Along all four other faces, a condition of zero normal deformation gradient is imposed, such that $(\text{Grad } \mathbf{u}(\mathbf{X}))^T \mathbf{n} = \mathbf{0}$.

These latter boundary conditions, known as *natural* boundary conditions in the finite-element literature, differ from the prescribed traction vector in (3.6). However, they are the standard choice of conditions for when Dirichlet conditions are not known or would otherwise “over-constrain” the system. Enforcing (3.6) directly would require adding forcing terms or traction conditions to the variational form, changing the formulation. The natural boundary conditions agree only in the trivial limit of small deformation, when $\gamma \rightarrow 0$. For small γ , one might hope, then, that the difference in deformation resulting from this change would be small. The following sections demonstrate that while this is true when considering the magnitude of the deformation, the resulting difference in energy is significant, with about 25% less total strain energy for the neo-Hookean case considered here. Furthermore, while all finite-element methods considered here converge to the same solution with moderate numbers of elements (thousands or tens-of-thousands), their behavior for small numbers of elements (hundreds or less) is dramatically different.

5 Deviation from simple shear

We first investigate the minimization of total strain energy under these “computational” boundary conditions through analytical calculation. Taking the simple shear deformation given in (3.1) and (3.2), we compute the first invariant of \mathbf{C} as $I_1 = \text{tr}(\mathbf{F}^T \mathbf{F}) = 3 + \gamma^2$, while $J = 1$. Since $J = 1$, the isochoric invariant, \bar{I}_1 , satisfies $\bar{I}_1 = I_1 = 3 + \gamma^2$, demonstrating that (4.1) and (4.2) are equal, and the energy associated with the Lagrange multiplier in either is uniformly zero. The strain energy of this simple shear (denoted by the superscript *SS*) is, then,

$$\pi_{FI}^{SS} = \int_{[0,1]^3} \frac{\mu}{2} [(3 + \gamma^2) - 3] + p(J - 1) dV = \frac{\mu \gamma^2}{2}. \tag{5.1}$$

Defining the reference volume, $V = \int_{[0,1]^3} dV$, and the strain energy per unit volume, $\Pi_{FI}^{SS} = \pi_{FI}^{SS}/V$, with $\gamma = 0.1$, we have $\Pi_{FI}^{SS} = 0.005\mu$.

To investigate the energy minimization, we next consider allowing simple variations in the displacements from those imposed in (3.1). To mimic the finite-element spaces used here, we consider a deformation that is always contained in the Q2P0 finite-element space on the unit cube. A prototypical deformation is chosen as

$$\begin{aligned} x_1 &= X_1 + \gamma X_3 + a(1 + 2X_1)X_3(1 - X_3), \\ x_2 &= X_2 + b(1 + 2X_2)X_3(1 - X_3), \\ x_3 &= X_3 + c(1 + 2X_1)X_3(1 - X_3), \end{aligned} \tag{5.2}$$

for unknowns parameters a , b , and c . The term $X_3(1 - X_3)$ ensures that the Dirichlet boundary conditions imposed on the $X_3 = 0$ and $X_3 = 1$ faces, both physically in (3.1) and computationally, are always satisfied. Minimizing the total strain energy from (4.1) then amounts to simply defining

$$\pi_{FI}^{Q2P0} = \min_{a,b,c,p} \int_{[0,1]^3} \frac{\mu}{2} [\hat{I}_1 - 3] + p(J - 1) dV, \tag{5.3}$$

where \hat{I}_1 is the first invariant of the Cauchy-Green tensor corresponding to (5.2). Taking $\gamma = 0.1$, the minimum of (5.3) is achieved when $a = -0.0011$, $b = -0.001$, $c = -0.021$ and $p = -0.995\mu$, giving $\Pi_{FI}^{Q2P0} = 0.00465\mu$, where again Π_{FI}^{Q2P0} is given per reference volume, $\Pi_{FI}^{Q2P0} = \pi_{FI}^{Q2P0}/V$. Plainly, this deformation achieves a smaller energy than that in (3.1), although we note that this deformation is non-physical in two regards. First, no traction forces are applied, allowing lower energy to be achieved at the expense of the simple shear deformation. Secondly, the incompressibility condition is no longer satisfied pointwise but, rather, only on average over the domain. While, in general, satisfying the incompressibility condition only on average can lead to significant non-physical properties of the finite-element solutions, numerical results in Section 6 show that such problems are relatively isolated when proper grid refinement is used.

A natural approach to improve the physical fidelity of the solution is to enrich the space for the Lagrange multiplier, p , in order to more strongly enforce the incompressibility condition. Following the above results, we then consider a minimization in a subset of the Taylor-Hood (Q2Q1) finite-element space on the unit cube, taking the same form for the deformation as given in (5.2), but allowing the Lagrange multiplier to vary in the space of trilinear functions. The resulting total strain energy is given by

$$\pi_{FI}^{Q2Q1} = \min_{a,b,c,p_i} \int_{[0,1]^3} \frac{\mu}{2} [\hat{I}_1 - 3] + (p_1 + p_2 X_1)(p_3 + p_4 X_2)(p_5 + p_6 X_3)(J - 1) dV. \quad (5.4)$$

However, it is apparent that the constant p minimization in (5.3) is performed over a subset of the minimization space in (5.4), fixing $p_2 = p_4 = p_6 = 0$. Thus, $\pi_{FI}^{Q2Q1} \leq \pi_{FI}^{Q2P0}$ and $\Pi_{FI}^{Q2Q1} \leq \Pi_{FI}^{Q2P0}$, showing that stronger enforcement of the incompressibility condition can only lower the minimum energy in this example. Thus, while these approaches clearly do not generate solutions that are guaranteed to be incompressible in a pointwise sense, we see that this should not be regarded as a fundamental flaw. As the computational results in Section 6 underscore, in combination with appropriate grid refinement, these approaches yield largely physically meaningful solutions that, nonetheless, vary in significant ways from the deformation gradient given in (3.2).

6 Numerical results

In this section, we compare results from the standard slightly compressible, hybrid slightly compressible, and fully incompressible formulations, generated by finite-element discretization over appropriate spaces. For the slightly compressible formulation, we use the implementation in Abaqus FEA (Dassault Systèmes Simulia, 2009), where we consider cubic elements with 27 nodes, representing the standard Q2 space for the displacements. For the hybrid formulation, we augment the Q2 displacements with Q1 hydrostatic pressure; we call the resulting element space Q2A to indicate the “augmented” formulations. In both the slightly compressible and hybrid formulations, we use the default value of $\kappa = 10^5\mu$, unless noted otherwise. For the fully incompressible formulation, we have developed an implementation for general material laws and boundary conditions in the finite-element package deal.II (Bangerth et al., 2007, 2013). We report results for Q2Q1 (Taylor-Hood), Q2P0, and stabilized Q1Q1 discretizations. We refer to Table 1 for a summary of these elements. Source code for the stable Q2Q1 and Q2P0 discretizations is available as supplementary material for this article.

Remark 1 *It was our intent to include numerical results for cubic elements with 8 nodes, representing standard Q1 (piecewise trilinear) finite-elements for the slightly compressible (Q1) and hybrid (Q1A) models. However, when processing the data from these numerical experiments, we noted that Abaqus FEA reported inconsistent results for the slightly compressible Q1 and Q1A models. Both models returned identical displacements that largely match those of the other methods reported here. However,*

we noted a significant disparity between the values of J at the integration nodes reported by Abaqus FEA (based on the undeformed, and deformed, representative volumes) and those computed directly from the deformation gradient at the integration nodes. Furthermore, there was disagreement between the deformation gradient computed from the displacement data and that provided directly by Abaqus FEA. The values of J computed from the deformation gradient coming from the displacements failed to match either of the other two values. Put simply, since Abaqus FEA uses black-box algorithms, we could not explain the discrepancies in these calculations. As a result, we have excluded data for these two test cases from the results in this section.

The deformation computed using Q2Q1 elements for the fully incompressible case is shown in Figure 2, where the color bars indicate the difference between the computed deformation and that of simple shear, computed as $x_i^h(X_1, X_2, X_3) - x_i(X_1, X_2, X_3)$ for $i = 1, 2, 3$, where x_i denotes the simple shear deformation given in (3.1), and $x_i^h = X_i + u_i^h$ is the computed deformation. We note that all discretizations converge to an equivalent solution. The most significant deviation is in the x_3 component.

Next, we compare solutions from all discretizations. Figure 3 shows the difference in the computed x_3 component between the midpoints of the faces $X_1 = 0$ and $X_1 = 1$ as the number of elements in the discretization is increased from 2^3 to 24^3 elements. For comparison, the simple shear solution has this difference as 0, since there is no deformation in the x_3 direction. Note that the results using the Q2 or Q1Q1 formulations coincide and vanish when 2^3 elements are used; in these cases, the computed displacement components represent the simple shear deformation. However, for all discretizations on all meshes larger than 12^3 elements, the numerical solutions are effectively identical in this measure. Considering the variation in the x_2 component, Figure 4 shows the difference from unit width in the computed solution along the face $X_1 = 1$, at the quarter-points $X_3 = 0.25$ and $X_3 = 0.75$. Again, for comparison, the simple shear solution has uniform unit width, so these deviations show the computed solutions varying from simple shear in this way. We note that, here, we see slower convergence to consistent solutions across all discretizations; only for the largest grids of 20^3 and 24^3 elements do we see numerical convergence.

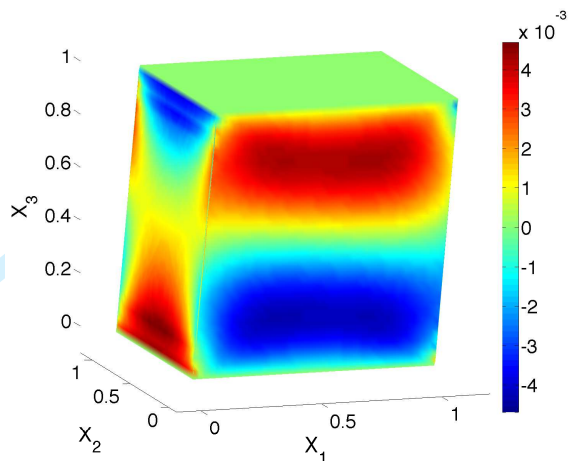
Figure 5 shows the computed strain energies (per total volume of reference configuration) for the various discretizations as the computational mesh is refined. All discretization approaches converge to similar solutions, as also seen in Figures 3 and 4. Deviations from the simple shear solution are small in the x_1 and x_2 components. Most notably, the cube does not maintain unit width, with widening near the corners defined by $X_1 = 0, X_3 = 1$ and $X_1 = 1, X_3 = 0$ and narrowing near the corners given by $X_1 = X_3 = 0$ and $X_1 = X_3 = 1$. The deviation in the x_3 component is more significant. Also interesting is the strong variation in computed deformations for small numbers of elements. All methods, except Q2P0, yield simple shear for the single element case. Figure 5 shows that with 2^3 elements, the Q2A and Q2Q1 solutions jump from simple shear to a deformation that is very close to the minimum strain energy, while Q2 and Q1Q1 yield the simple shear solution for 2^3 elements, but no larger. All methods, except Q2A and Q2Q1, converge relatively slowly to the minimal strain energy, as reflected in Figures 3, 4, and 5. We note that the minimal strain energy achieved as the mesh size is decreased is significantly below that of the simple shear solution.

Seeing that, as the number of elements increase, these methods approach a solution that is not the simple shear solution raises the question of whether or not the computational solution is truly incompressible, or only approximately so. Figure 6 presents the maximum and minimum values of J over the entire body for each approach, varying the number of elements in the discrete mesh. Considering the performance with respect to method, we see that all of the fully incompressible approaches, as well

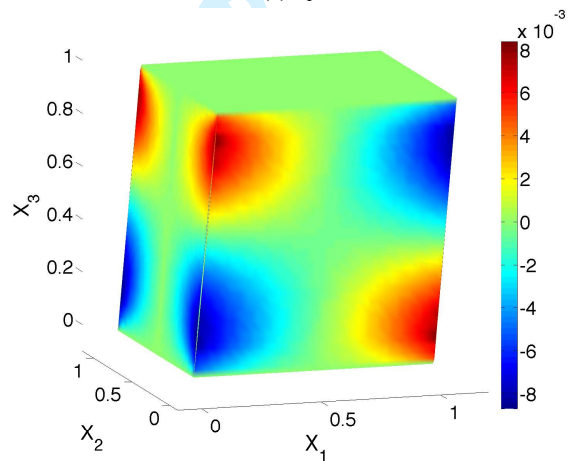
1
2
3
4
5
6
7
8
9
10
11
12
13
14
15
16
17
18
19
20
21
22
23
24
25
26
27
28
29
30
31
32
33
34
35
36
37
38
39
40
41
42
43
44
45
46
47
48
49
50
51
52
53
54
55
56
57
58
59
60



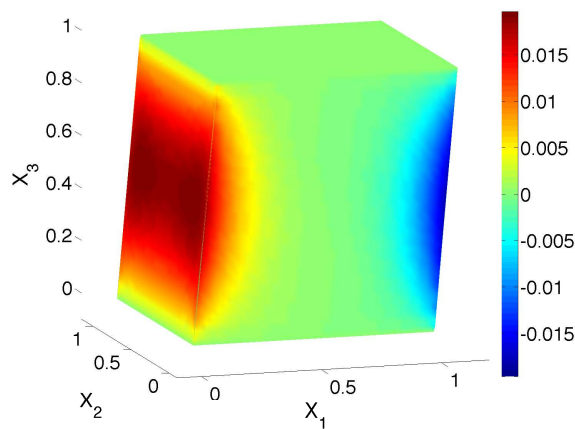
FEM for incompressible shear



(a) x_1 deviation



(b) x_2 deviation



(c) x_3 deviation

FIG. 2: Deviation (given per cube edge reference length) from simple shear deformation in each component for the fully incompressible numerical case, discretized using Q2Q1 elements on a 20^3 grid.



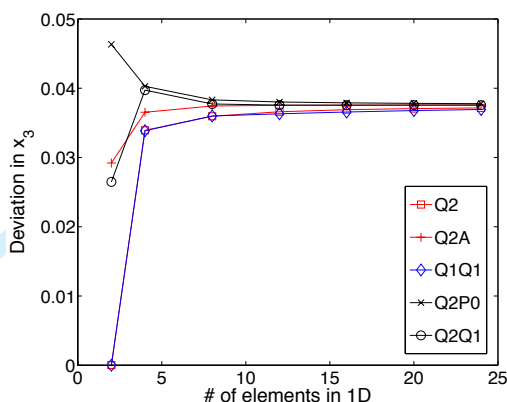
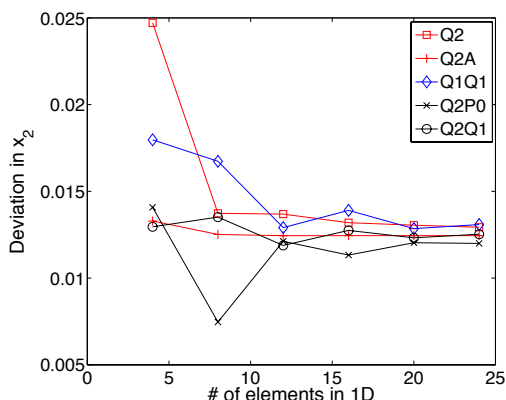
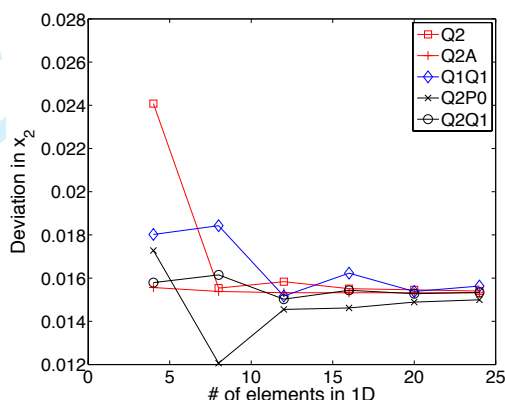


FIG. 3: Difference (given per cube edge reference length) in the x_3 component of the finite-element solutions between midpoints of the faces $X_1 = 0$ and $X_1 = 1$, computed as $x_3(0, 1/2, 1/2) - x_3(1, 1/2, 1/2)$.



(a) Deviation from unit length in the x_2 direction for $X_3 = 0.25$



(b) Deviation from unit length in the x_2 direction for $X_3 = 0.75$

FIG. 4: Deviation from unit length (given per cube edge reference length) in the x_2 component of the finite-element solutions along the $X_1 = 1$ face, computed as $x_2(1, 0, X_3) - x_2(1, 1, X_3) - 1$.

as the hybrid approach, lead to much larger variations in J than the standard slightly compressible approach does with $\kappa = 10^5 \mu$. Considering the forms of the strain-energy functional, the positive penalty term used in the slightly compressible formulation given in (4.3) explains the strict adherence to the constraint seen in the Q2 results in Figure 6.

In Figure 7, we explore the dependency of the results for Q2 on the ratio, κ/μ , noting significant deviations from $J = 1$ for small κ/μ in the figure at left, and that $|J - 1|$ scales roughly as $10^{-\mu/\kappa}$ in the figure at right. Each of the other approaches augments the isochoric strain energy with additional terms, ensuring that $J = 1$ in some averaged sense, but not necessarily pointwise. We also note that with $\kappa/\mu = 10^6$, we see the onset of volumetric locking already, with no convergence in our solution past 12

FEM for incompressible shear

19 of 27

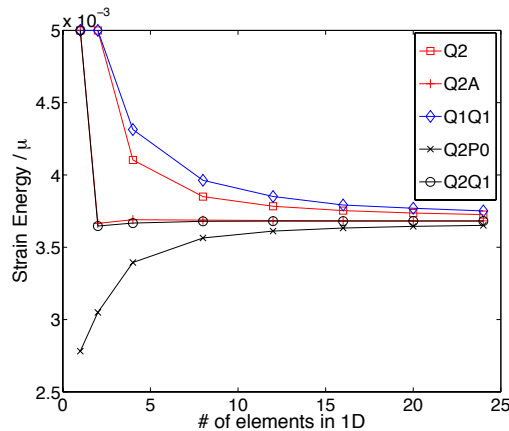


FIG. 5: Strain energy (per total volume of reference configuration) of the finite-element solutions as a function of grid refinement. Note that a strain energy of $(5 \times 10^{-3}) \mu$ corresponds to the analytical simple shear deformation.

elements in each direction.

To get a better understanding of this deviation, Figure 8 shows the pointwise values of J on the faces of the cube for the Q2, Q2Q1, and Q2A discretizations, and how these change with refinement from 8^3 to 16^3 elements. In Figures 8a and 8b, we show the deviation from $J = 1$ for the Q2 discretization with $\kappa = \mu$, chosen to emphasize the variations for small κ/μ in this formulation. Here, we see deviations from unity that are large near the four edges experiencing the largest deformation, but that these deviations change only slightly with grid refinement. Figures 8c and 8d show that, in contrast, the variations for Q2Q1 are strongly localized to the $X_1 = 0$ and $X_1 = 1$ faces of the cube, and that they become more localized to the top and bottom edges of these faces when the mesh is refined. Similar behavior is seen in Figures 8e and 8f for the Q2A discretization. We note that similar results to those for Q2Q1 are obtained for other choices of finite-element spaces using the fully incompressible formulation, and that results similar to Q2 are obtained for other values of κ/μ , albeit with smaller variations as κ/μ increases. As discussed above, the observed growth in the maximum pointwise values of J with grid refinement in the mixed formulations does not directly contradict the standard finite-element error analysis, so long as the volume over which J is significantly different from 1 contracts faster than the pointwise values grow. This is precisely what we see in these results.

It is clear that the best physical fidelity in these solutions arises from the Q2 slightly compressible approach with large κ/μ . If the computational cost of generating solutions with this approach was comparable to all others, then the path forward would be clear. Figure 9 shows, however, that there is great variation in the computational costs, both with formulation and finite-element strategy and with κ/μ for the standard slightly compressible approach. At the left of Figure 9, we see how the number of linearization steps needed varies with method. Using the standard slightly compressible model with $\kappa = 10^5 \mu$ is prohibitively expensive, with number of linearization steps growing with problem size. This is emphasized by the right side of Figure 9, which shows that this growth increases with κ/μ , to the point of a scheme that is no longer convergent for $\kappa = 10^6 \mu$ and a moderate number of elements (as expected from the phenomenon of volumetric locking). The second conclusion from the left figure

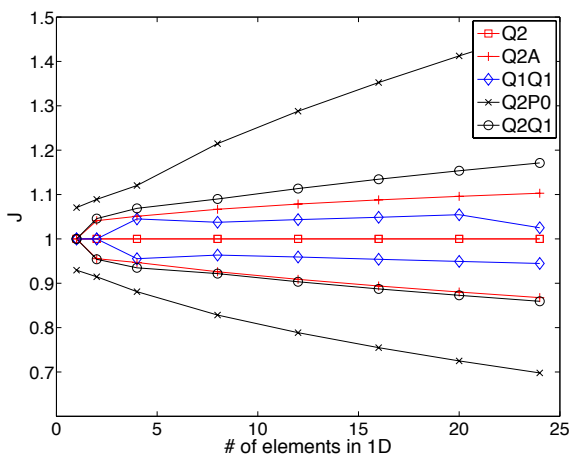
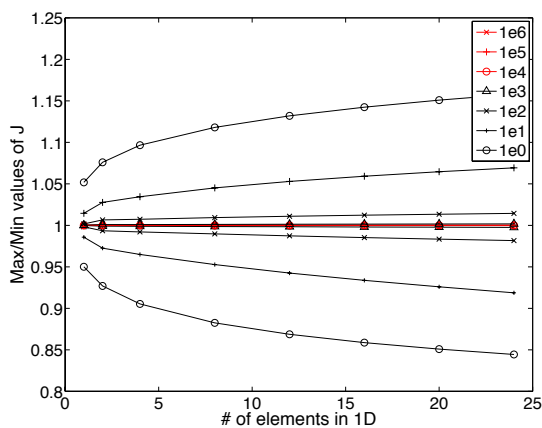
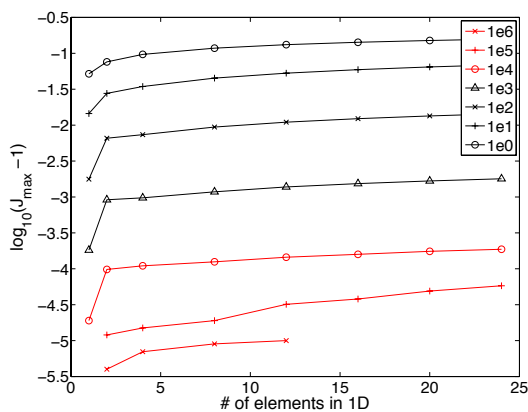


FIG. 6: Maximum and minimum values of J at the quadrature nodes of the discretization as a function of finite-element approach and varying mesh size.



(a) Varying κ/μ for Q2



(b) Logarithmic scaling of deviation of maximum value of J with varying κ/μ , for Q2

FIG. 7: Minimum and maximum values of J at quadrature nodes of the discretization for a standard slightly compressible model with Q2 elements. At left, the maximum and minimum values over the mesh. At right, data for the maximum values on a logarithmic scale.

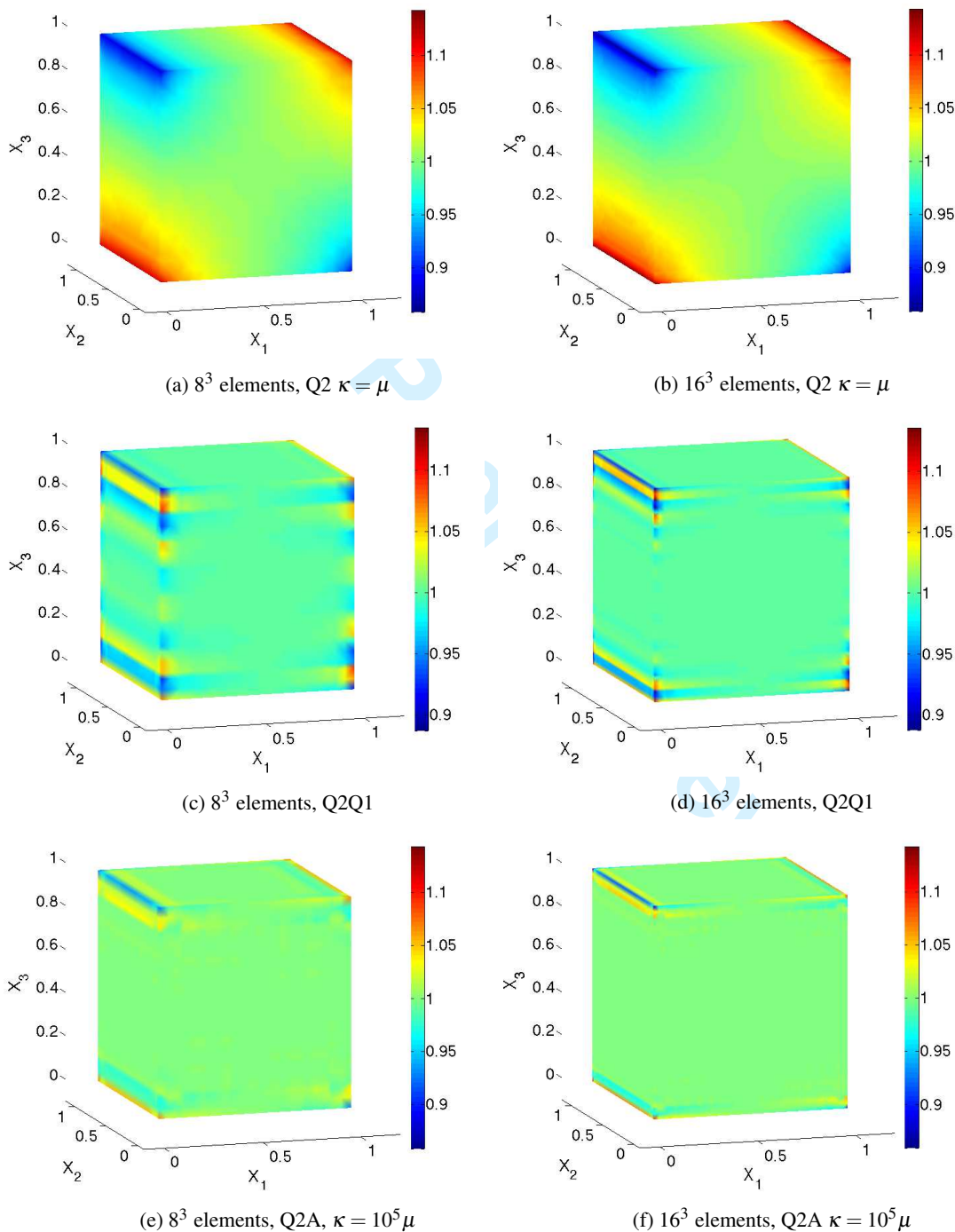


FIG. 8: Value of J at the quadrature nodes (projected to the surface of the cube) for Q2, Q2Q1, and Q2A discretizations on 8^3 and 16^3 meshes.

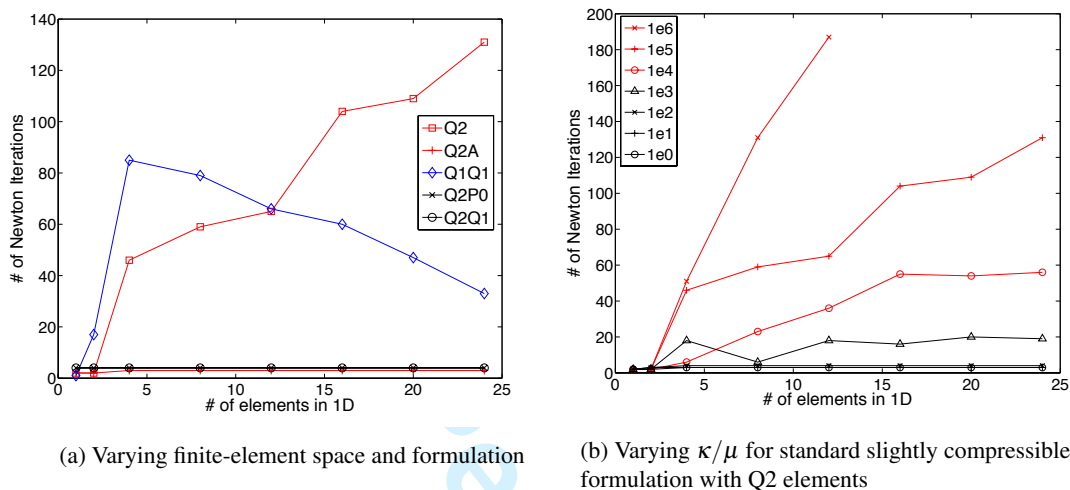


FIG. 9: Number of linearizations (Newton iterations) to reach convergence (measured as small non-linear residual). At left, compared across formulations and finite-element spaces. At right, compared across κ/μ for the standard slightly compressible formulation with Q2 elements.

is that the stabilized Q1Q1 fully incompressible formulation suffers greatly in comparison to the stable methods, although the number of linearization steps for this approach is clearly decreasing as problem size increases. In contrast, all of the remaining augmented formulations (both fully incompressible and hybrid slightly compressible) yield a solution after only a handful of linearizations.

While the numerical results presented above are specific to the Neo-Hookean material law of Equation (2.9), nearly identical results were obtained for a Mooney-Rivlin material law. Clearly, variations in the computed deformations could be achieved by considering more complex material laws, such as those in Destrade et al. (2012a,b); Horgan and Murphy (2010, 2011); Mihai and Goriely (2011) and Rashid et al. (2013); nonetheless, the question of pointwise satisfaction of the incompressibility constraint within these models remains an important one, that is partly illuminated by the results above.

7 Discussion

It is widely regarded that there are numerous challenges to both the theory and practice of generating numerical solutions to problems of incompressible nonlinear elasticity in three dimensions. In this paper, we aim to gain some insight into these problems from the point-of-view of understanding the interplay between the mathematical and computational models of simple shear of a homogeneous cube. Three mathematical formulations are considered, two following from the slightly compressible viewpoint, along with a fully incompressible approach. Suitable finite-element based discretizations are posed for each.

Contrary to expectations, simple shear does not provide an example where an analytical solution can be used to check the accuracy of the resulting finite-element discretizations, due to the mismatch between the boundary conditions and forces needed to maintain the simple shear solution and those that are naturally implemented in the finite-element framework. However, highlighting the utility of

REFERENCES

23 of 27

numerical approaches to obtain accurate results, a computational study reveals that all methods converge to a solution that is qualitatively the same, with out-of-plane deformation.

Despite a misleading nomenclature, it is clear that the fully incompressible approach leads to discrete representations where incompressibility is enforced only in an average sense, leading to large pointwise variations in the volume ratio, J , for these solutions. The slightly compressible formulations lead to solutions that are more faithful to the incompressibility constraint for large bulk moduli; however, the standard slightly compressible formulation clearly suffers from effects of volumetric locking in this parameter range. Thus, since the offending variations of the fully incompressible approach are contained within only a small fraction of the total volume (which decreases with grid refinement as required by finite-element error analysis), it is difficult to say which approach is truly the preferred choice. When balanced against the expected computational cost of solving the resulting nonlinear and linearized systems, it is clear that the use of mixed finite-element methods, either for the hybrid slightly compressible or fully incompressible approaches, is highly preferable. To further resolve this question, close study of these computational costs and design of effective preconditioning strategies is needed.

Acknowledgements

The material is based upon work by D. Han supported by the United States–Israel Binational Science Foundation (BSF) under the Research Grant 2008419, and by C. Paetsch supported by the National Science Foundation IGERT Grant DGE-1144591.

References

- Adams, S. and Cockburn, B. 2005. A mixed finite element method for elasticity in three dimensions. *J. Sci. Comput.* 25:515–521.
- Arnold, D. N., Brezzi, F., and Douglas, Jr., J. 1984*a*. PEERS: a new mixed finite element for plane elasticity. *Japan J. Appl. Math.* 1:347–367.
- Arnold, D. N., Brezzi, F., and Fortin, M. 1984*b*. A stable finite element for the Stokes equations. *Calcolo* 21:337–344 (1985).
- Arnold, D. N., Falk, R. S., and Winther, R. 2007. Mixed finite element methods for linear elasticity with weakly imposed symmetry. *Math. Comp.* 76:1699–1723.
- Arnold, D. N. and Winther, R. 2002. Mixed finite elements for elasticity. *Numer. Math.* 92:401–419.
- Auricchio, F., Beirão da Veiga, L., Lovadina, C., Reali, A., Taylor, R., and Wriggers, P. 2013. Approximation of incompressible large deformation elastic problems: some unresolved issues. *Computational Mechanics* 52:1153–1167.
- Bangerth, W., Hartmann, R., and Kanschat, G. 2007. deal.II – a general purpose object oriented finite element library. *ACM Trans. Math. Softw.* 33:24/1–24/27.
- Bangerth, W., Heister, T., Heltai, L., Kanschat, G., Kronbichler, M., Maier, M., Turkcsin, B., and Young, T. D. 2013. The deal.ii library, version 8.0. arXiv preprint <http://arxiv.org/abs/1312.2266>.
- Belytschko, T., Liu, W. K., and Moran, B., 2000. *Nonlinear finite elements for continua and structures*. Wiley.

- Belytschko, T., Ong, J. S. J., Liu, W. K., and Kennedy, J. M. 1984. Hourglass control in linear and nonlinear problems. *Computer Methods in Applied Mechanics and Engineering* 43:251–276.
- Boffi, D., Brezzi, F., and Fortin, M., 2013. *Mixed finite element methods and applications*, volume 44 of *Springer Series in Computational Mathematics*. Springer, Heidelberg.
- Bonet, J. and Wood, R. D., 2008. *Nonlinear continuum mechanics for finite element analysis*. Cambridge University Press.
- Bose, K. and Dorfmann, A. 2009. Computational aspects of a pseudo-elastic constitutive model for muscle properties in a soft-bodied arthropod. *International Journal of Non-Linear Mechanics* 44:42–50.
- Braess, D., 2007. *Finite elements*. Cambridge University Press, Cambridge, third edition.
- Brenner, S. C. and Scott, L. R., 2002. *Mathematical Theory of Finite Element Methods*. Springer, second edition.
- Chi, S.-W., Chen, J.-S., and Hu, H.-Y. 2014. A weighted collocation on the strong form with mixed radial basis approximations for incompressible linear elasticity. *Computational Mechanics* 53:309–324.
- Ciarlet, P. G., 1988. *Mathematical elasticity, vol 1: three-dimensional elasticity*. North Holland, Amsterdam.
- Crisfield, M. A., 1991. *Non-linear finite element analysis of solids and structures*. Wiley.
- Dassault Systèmes Simulia, 2009. *Abaqus FEA 6.9*. Providence RI, USA.
- deBotton, G., Bustamante, R., and Dorfmann, A. 2013. Axisymmetric bifurcations of thick spherical shells under inflation and compression. *International Journal of Solids and Structures* 50:403–413.
- Destrade, M., Gilchrist, M., Motherway, J., and Murphy, J. 2012a. Slight compressibility and sensitivity to changes in Poisson’s ratio. *International Journal for Numerical Methods in Engineering* 90:403–411.
- Destrade, M., Murphy, J., and Saccomandi, G. 2012b. Simple shear is not so simple. *International Journal of Non-Linear Mechanics* 47:210 – 214.
- Doghri, I., 2000. *Mechanics of deformable solids*. Springer-Verlag, Berlin. Linear, nonlinear, analytical and computational aspects.
- Dohrmann, C. R. and Bochev, P. B. 2004. A stabilized finite element method for the Stokes problem based on polynomial pressure projections. *Internat. J. Numer. Methods Fluids* 46:183–201.
- Dorfmann, A. L. and Ogden, R. W., 2014. *Nonlinear Theory of Electroelastic and Magnetoelastic Interactions*. Springer.
- Ehlers, W. and Eipper, G. 1998. The simple tension problem at large volumetric strains computed from finite hyperelastic material laws. *Acta Mechanica* 130:17–27.

REFERENCES

25 of 27

- Elman, H., Silvester, D., and Wathen, A., 2005. Finite Elements and Fast Iterative Solvers: with Applications in Incompressible Fluid Dynamics. Oxford University Press, Oxford.
- Fu, Y. B. and Ogden, R. W., 2001. Nonlinear elasticity: theory and applications. University Press, Cambridge.
- Gent, A. N., Suh, J. B., and Kelly, III, S. G. 2007. Mechanics of rubber shear springs. International Journal of Non-Linear Mechanics 42:241–249.
- Holzappel, G. A., 2001. Nonlinear solid mechanics: a continuum approach for engineering. John Wiley & Sons, Chichester.
- Horgan, C. O. and Murphy, J. G. 2007. Constitutive models for almost incompressible isotropic elastic rubber-like materials. Journal of Elasticity 87:133–146.
- Horgan, C. O. and Murphy, J. G. 2009a. Compression tests and constitutive models for the slight compressibility of elastic rubber-like materials. International Journal of Engineering Science 47:1232–1239.
- Horgan, C. O. and Murphy, J. G. 2009b. On the volumetric part of strain-energy functions used in the constitutive modeling of slightly compressible solid rubbers. International Journal of Solids and Structures 47:3078–3085.
- Horgan, C. O. and Murphy, J. G. 2009c. Constitutive modeling for moderate deformations of slightly compressible rubber. Journal of Rheology 53:153–168.
- Horgan, C. O. and Murphy, J. G. 2010. Simple shearing of incompressible and slightly compressible isotropic nonlinearly elastic materials. Journal of Elasticity 98:205–221.
- Horgan, C. O. and Murphy, J. G. 2011. Simple shearing of soft biological tissues. Proceedings of the Royal Society A-Mathematical Physical and Engineering Sciences 467:760–777.
- Hughes, T. J. R. 1977. Equivalence of finite elements for nearly incompressible elasticity. Journal of Applied Mechanics 44:181–183.
- Hughes, T. J. R. 1980. Generalization of selective integration procedures to anisotropic and nonlinear media. International Journal for Numerical Methods in Engineering 15:1413–1418.
- Hughes, T. J. R. and Malkus, D. S., 1983. A general penalty/mixed equivalence theorem for anisotropic incompressible elements *in N*. Atluri, R. Gallager, and O. Zienkiewicz, eds. Hybrid and Mixed Finite Element Methods. Wiley.
- Malkus, D. S. and Hughes, T. J. R. 1978. Mixed finite element methods - reduced and selective integration techniques: A unification of concepts. Computer Methods in Applied Mechanics and Engineering 15:63–81.
- Merodio, J. and Neff, P. 2006. A note on tensile instabilities and loss of ellipticity for a fiber reinforced nonlinearly elastic material. Arch. Mech. 58:293–303.
- Merodio, J. and Ogden, R. W. 2003. Instabilities and loss of ellipticity in fiber-reinforced compressible non-linearly elastic solids under plane deformation. Int. J. Solids Struct. 40:4707–4727.

- Mihai, L. A. and Goriely, A. 2011. Positive or negative Poynting effect? the role of adscitious inequalities in hyperelastic materials. *Proceedings of the Royal Society A-Mathematical Physical and Engineering Sciences* 467:3633–3646.
- Ogden, R. W. 1972*a*. Large deformation isotropic elasticity - correlation of theory and experiment for compressible rubberlike solids. *Proceedings of the Royal Society of London Series A-Mathematical and Physical Sciences* 328:567–583.
- Ogden, R. W. 1972*b*. Large deformation isotropic elasticity - on the correlation of theory and experiment for incompressible rubberlike solids. *Proceedings of the Royal Society of London Series A-Mathematical and Physical Sciences* 326:565–584.
- Ogden, R. W. 1976. Volume changes associated with deformation of rubber-like solids. *Journal of the Mechanics and Physics of Solids* 24:323–338.
- Ogden, R. W. 1978. Nearly isochoric elastic deformations - application to rubber-like solids. *Journal of the Mechanics and Physics of Solids* 26:37–57.
- Ogden, R. W., 1997. *Non-linear elastic deformations*. Dover Publications, New York.
- Paetsch, C. and Dorfmann, A. 2013. Non-linear modeling of active biohybrid materials. *International Journal of Non-Linear Mechanics* 56:105–114.
- Peng, S. H. and Chang, W. V. 1997. A compressible approach in finite element analysis of rubber-elastic materials. *Computers & Structures* 62:573–593.
- Rashid, B., Destrade, M., and Gilchrist, M. D. 2013. Mechanical characterization of brain tissue in simple shear at dynamic strain rates. *Journal of the Mechanical Behavior of Biomedical Materials* 428:71–85.
- Rivlin, R. S. 1948. Large elastic deformations of isotropic materials . IV. Further developments of the general theory. *Philosophical Transactions of the Royal Society of London Series A-Mathematical And Physical Sciences* 241:379–397.
- Rossi, S., Ruiz-Baier, R., Pavarino, L. F., and Quarteroni, A. 2012. Orthotropic active strain models for the numerical simulation of cardiac biomechanics. *Int. J. Numer. Methods Biomed. Eng.* 28:761–788.
- Ruiz-Baier, R., Gizzi, A., Rossi, S., Cherubini, C., Laadhari, A., Filippi, S., and Quarteroni, A. 2013. Mathematical modelling of active contraction in isolated cardiomyocytes. *Mathematical Medicine and Biology* .
- Simo, J. C. and Taylor, R. L. 1991. Quasi-incompressible finite elasticity in principal stretches. Continuum basis and numerical algorithms. *Comput. Methods Appl. Mech. Engrg.* 85:273–310.
- Simo, J. C., Taylor, R. L., and Pister, K. S. 1985. Variational and projection methods for the volume constraint in finite deformation elasto-plasticity. *Computer Methods in Applied Mechanics and Engineering* 51:177–208.
- Spencer, A. J. M., 1971. Theory of invariants. Pages 239–353 in A. C. Eringen, ed. *Continuum physics*, volume 1. Academic Press, New York.

1
2
3
4
5
6
7
8
9
10
11
12
13
14
15
16
17
18
19
20
21
22
23
24
25
26
27
28
29
30
31
32
33
34
35
36
37
38
39
40
41
42
43
44
45
46
47
48
49
50
51
52
53
54
55
56
57
58
59
60



REFERENCES

27 of 27

Truesdell, C. and Noll, W., 1965. The nonlinear field theories of mechanics *in* S. Flügge, ed. Handbuch der Physik, Vol III/3. Springer, Berlin.

Wu, C. T., Hu, W., and Chen, J. S. 2012. A meshfree-enriched finite element method for compressible and near-incompressible elasticity. *Internat. J. Numer. Methods Engrg.* 90:882–914.

For Peer Review

